

Stability and superconductivity of TiPH_n ($n = 1-8$) under high pressure

Xue Guo,^a Ru-Lin Wang,^a Hai-Liang Chen,^a and Wen-Cai Lu^{a,b,}
K. M. Ho^c and C. Z. Wang^c*

^aCollege of Physics and State Key Laboratory of Bilological Polysaccharide Fiber Forming and Ecological Textile, Qingdao University, Qingdao, Shandong 266071, P. R. China

^bInstitute of Theoretical Chemistry, Jilin University, Changchun, Jilin 130021, P. R. China

^cAmes Laboratory–US DOE and Department of Physics and Astronomy, Iowa State University, Ames, Iowa 50011, USA

*Email: wencailu@jlu.edu.cn

Abstract

Titanium exhibits high affinity to hydrogen and the Ti-H compounds are thermodynamically stable. We introduced the Ti elements in the P-H compounds to deal with the thermodynamic-instability issue of the P-H compounds. In this work, ternary hydrogen-rich compounds TiPH_n ($n = 1-8$) were studied and calculated using the density function theory (DFT) method. The results showed that the TiPH_4 and TiPH_8 had high superconducting critical temperatures (T_c) as well as better stability. Among TiPH_n ($n = 1-8$), the TiPH and TiPH_4 were most stable at 50-200 and 250-300 GPa, respectively. For the R-3m- TiPH_4 structure, the predicted T_c 's are 52 and 62 K at 100 and 250 GPa, respectively, and its larger Young's modulus suggested that it might be potentially synthesized in experiment.

Keywords: TiPH_n hydride, Ti-H hydride, P-H hydride, superconductivity, stable structure at high pressure

1. Introduction

It has been proposed, based on the Bardeen Cooper Schrieffer (BCS) theory^[1], that highly compressed solid hydrogen^[2] and hydrogen-rich compounds^[3] can possess high superconducting transition temperatures (T_c) due to the high vibration frequencies of hydrogen atoms in these materials. Recently, experimental studies on H_2S , PH_3 and LaH_{10} ^[4-6], and many theoretical studies on H_3S , YH_{10} , LaH_{10} , CaH_6 , SiH_4 , and B_2H_6 ^[7-11], etc. have demonstrated the superconductivity in these H-rich materials under high pressure.

The theoretical and experimental results indicated that many binary H-rich materials at high pressure such as H_3S ^[7], YH_{10} ^[8], LaH_{10} ^[8], CaH_6 ^[9], SiH_4 ^[10] and MgH_6 ^[12], etc. exhibit high T_c . One of the representative examples is H_2S/H_3S , for which the experimental reported T_c is 203 K at 155 GPa and it was also suggested that the high T_c may be resulted from the decomposed product H_3S .^[5] Before this experiment, the theoretical study had predicted that the H_3S Im-3m structure had a T_c as high as 191-204 K at 200 GPa.^[7] Also, the theoretical study showed that H_2S could only be stable below 43 GPa, and when the pressure is above 43 GPa the most stable structure is the H_3S Im-3m phase until 300 GPa, indicating that H_2S would decompose into H_3S plus S above 43 GPa.^[7] For yttrium hydrides, it was theoretically predicted that YH_6 has a very high T_c of 251-264 K at 120 GPa,^[13] and YH_{10} , had a very high T_c of 305-326 K at 250 GPa.^[8] LaH_{10} had a very high T_c of 274-286 K at 210 GPa.^[8] In addition, MgH_6 and CaH_6 were theoretically predicted to have very high T_c of ~260 K at 300 GPa,^[12] and 200-235 K at 150 GPa,^[9] respectively.

For the SiH₄ compounds mentioned above, it was found to decompose at room temperature above 50 GPa and can react with other metals from the diamond anvil cell to form compounds including PtH.^[14] This conclusion was also confirmed theoretically that the T_c of PtH is in good agreement with the experimental data of T_c.^[15-16] GeH₄ was theoretically predicted to achieve superconductivity at 20 GPa with a T_c of 40 K.^[17-18] Moreover, actinide-based hydrides have also attracted much attention, e.g., the superconductivity of ThH₁₀ was theoretically studied and the predicted T_c was 194 K at 100 GPa.^[19]

There are a few studies on ternary hydride superconductors, e.g., Fe₂SH₃ was theoretically predicted to be stable at 100 GPa, with a very small T_c of only ~ 0.3 K at 173 GPa.^[20] Besides, theoretical predictions showed that Ba(AuH₂)₂ and Sr(AuH₂)₂ were stable at 1 atm and had the T_c of 30 and 10 K, respectively.^[21] The theoretical study on MgSiH₆, showed that it has a T_c of ~ 63 K at 250 GPa.^[22] Recently, Fan *et al.* studied theoretically the superconductivity of H₃S_xP_{1-x}, H₃P_xS_{1-x} and H₃Cl_xS_{1-x} at 200 GPa using virtual crystal approximation (VCA), and found that the T_c (197 K) of H₃P_{0.15}S_{0.085}, was the highest.^[23] Also, it was found in the experiment that the T_c in the hydrogen rich BaReH₉ was ~7 K at above 100 GPa.^[24]

For phosphorous compounds, a systematic theoretical study on PH_n (n = 1-6) showed that the T_c of the monoclinic phase C2/m of PH₃ reached about 100 K at 200 GPa, and two C2/m and I4/mmm structures of PH₂ had T_c of about 76 and 70 K, respectively, at 200 GPa.^[25-27] Meanwhile, the T_c of PH₃ was reported experimentally to be 103 K at 207 GPa.^[4] However, the P-H compounds are unstable and exhibit a

tendency of decomposition to P and H₂ at high pressures.^[25] In recent experimental studies, the presence of the Ti-H compounds were reported, and the T_c of TiH_{2.74} was predicted to be 4 K.^[28] Although the Ti-H compounds did not have high T_c, they can be stabilized at normal pressure, because Ti has a very high affinity to hydrogen, acting as a typical hydride forming agent. As a result, the titanium hydride had brittle phases, and hydrogen embrittlement can lead to premature failure of titanium alloys.^[28] The Ti-H compounds have high stability, but relatively low T_c. On the other hand, as mentioned above, the P-H compounds had been experimentally shown to have high T_c, but they were thermodynamically unstable, which affects the applicability of the P-H superconductors, thus in our study, Ti was introduced to the P-H systems, the high affinity of Ti to H would bring better stability of the Ti-P-H compounds.

2. Computational details

The low-enthalpy structures of TiPH_n (n = 1-8) at high pressure were searched by genetic algorithm (GA)^[29-31] combined with structural optimizations using density functional theory (DFT). Perdew-Burke-Ernzerh (PBE) exchange-correlation energy functional^[32-33] and ultrasoft pseudopotentials, implemented in the CASTEP code^[34] are employed. It had been shown that the GA search is very successful in predicting crystalline structures.^[35-39] The GA search of low-enthalpy structures of TiPH_n (n = 1-8) were performed at 200 GPa, with a GA pool containing 80 candidate structures. Then the low-enthalpy structures from the GA search were re-optimized with high precision at the pressure range 50 - 300 GPa, with a 800 eV for the kinetic energy

cutoff for plane wave basis and a Monkhorst-Pack k-point sampling resolution of $2\pi \times 0.03 \text{ \AA}^{-1}$.

The phonon spectra and electron-phonon coupling (EPC) parameters were calculated using the Quantum-Espresso (QE)^[40] code with the DFT-PBE method and ultrasoft pseudopotentials. In QE,^[40] we re-optimized structures with an energy cutoff of 816 eV and k meshes of $16 \times 16 \times 16$, $16 \times 16 \times 4$, $12 \times 12 \times 8$, $16 \times 16 \times 4$, $12 \times 12 \times 4$, $12 \times 16 \times 8$, $12 \times 20 \times 12$, and $12 \times 16 \times 8$ for TiPH₁, TiPH₂, TiPH₃, TiPH₄, TiPH₅, TiPH₆, TiPH₇, TiPH₈, respectively. For TiPH₄, the phonon dispersions and electron-phonon couplings and the T_c were calculated by a q mesh of $8 \times 8 \times 2$.

3. Results and discussion

3.1 Structural stability of TiPH_n (n = 1-8)

The stable structures of TiPH_n (n = 1-8) were investigated at the pressure range of 50-300 GPa. Unlike binary hydrides, there are many decomposition paths for ternary compounds. Due to the instability of hydrogen phosphide, we don't need to consider the decomposition paths to P-H compounds. In the experiment, the stoichiometric ratio of the Ti-H compound was found to be TiH_{2.74}.^[41] We estimated the stabilities of TiH₂ and TiH₃ and found that TiH₂ is more stable than TiH₃. Therefore, we analyzed the Ti-P-H compound stabilities by two decomposition paths: TiPH_n → TiH₂ + P + (n-2)H and TiPH_n → TiP + nH. Among the two paths, the first one TiPH_n → TiH₂ + P + (n-2)H corresponds to a smaller enthalpy difference and thus more favorable for TiPH₂₋₈ decompositions.

The structural stabilities of the TiPH_n compounds were estimated by the calculated enthalpies of formation per atom (ΔH 's). The most stable structures obtained for TiPH_{1-8} are P3m1, P-6m2, R3m, R-3m, I-4m2, Cm, P3, and C2/m structures, respectively, at 50-300 GPa. For each TiPH_n compound, there is no phase transition occurs in the pressure range of 50-300 GPa. The TiPH_2 -P-6m2, TiPH_3 -R3m and TiPH_7 -P3 structures were found to be dynamically unstable, we therefore replaced them with TiPH_2 -R-3m, TiPH_3 -Amm2 and TiPH_7 -Cm, respectively, in phonon and T_c calculations. The crystal structures of TiPH -P3m1, TiPH_2 -R-3m, TiPH_4 -R-3m and TiPH_8 -C2/m at 250 GPa were shown in Figure 1, and the others were shown in Figure S1.

When calculating enthalpy differences, the most stable phases of H were taken as P63/m at 50-100 GPa, C2/c at 150-250 GPa and Cmca at 300 GPa,^[42] and those for P were Pm-3m at 50-100 GPa, P6/mmm at 150-200 GPa, Im-3m at 250-300 GPa.^[43-47] The structures for TiP were taken as Cmcm at 50-200 GPa, and Cmmm at 250-300 GPa, and those for TiH_2 were I4/mmm at 50 GPa, P4/nmm at 100-250 GPa, and P2₁/m at 300 GPa.^[48] The enthalpy differences of TiPH_n ($n = 1-8$) related to the two decomposition paths were displayed in Figures 2 (a) and (b).

Figure 2 (a) displays the stability of TiPH_n ($n = 1-8$) relative to decomposition path $\text{TiPH}_n \rightarrow \text{TiP} + n\text{H}$. In the pressure range of 50-200 GPa, TiPH is the most stable structure. According to the convex hull diagram (Figure 2 (a)), TiPH_4 becomes stable above 100 GPa and turns to be most stable at 250-300 GPa, TiPH_2 becomes stable above 250 GPa, and TiPH_8 can be stabilized above 200 GPa. Figure 2 (b) shows the

formation enthalpy of TiPH_n ($n = 2-8$) relative to $\text{TiH}_2 + \text{P} + (n-2)\text{H}$ for the most favorable structures for each composition. When the pressures was lower than 50 GPa, the structures of all TiPH_n ($n = 2-8$) systems are thermodynamically unstable, and TiPH_4 becomes stable from 100 GPa on. With the pressure increased to 200-300 GPa, TiPH_4 maintains to be the most stable stoichiometry, and also TiPH_8 becomes stable, while TiPH_3 , TiPH_5 , TiPH_6 and TiPH_7 are metastable by the convex hull diagram (Figure 2 (b)).

In order to further investigate the stability of the Ti-P-H compounds, the trigonometric phase diagram is employed to analyze the enthalpy values under different pressures, as shown in Figure 3. And the three vertices represent the enthalpy values for the pure titanium, phosphorus and hydrogen, respectively. We only plot the corresponding compounds with the lower enthalpy compared with the potential energy surface formed by the three monomers after unitization. In other words, the trigonometric phase diagram shows the stable structures under the corresponding pressure, indicating that the stability of TiPH_4 and TiPH_8 in the pressure range of 200-300 GPa, which is in agreement with the results from enthalpy difference analyses by the two decomposition paths in Figure 2.

3.2 Electronic properties and superconductivity of TiPH_2 , TiPH_4 and TiPH_8

For TiPH_2 , TiPH_4 and TiPH_8 , we further studied their electronic, dynamic and mechanical properties, as well as superconducting properties. To determine whether TiPH_2 -R-3m, TiPH_4 -R-3m and TiPH_8 -C2/m are metals under a given pressure, the electronic band structures and projected density of states (PDOSs) of TiPH_2 -R-3m,

TiPH₄-R-3m and TiPH₈-C2/m were calculated, e.g., their band structures at 250 GPa as shown in Figure 4. The overlap between conduction bands and valence bands at the Fermi level (N_F) show their metallic character. The overlap of energy bands at Fermi level will directly affect the prediction results of T_c .

Next, we calculated the phonon dispersion curves and phonon density of states (PHDOSs) of TiPH₂-R-3m at 250 GPa, TiPH₄-R-3m at 100 and 250 GPa, and TiPH₈-C2/m at 250 GPa to determine their dynamic stabilities. The results indicate that their phonon dispersion curves have no imaginary frequency (Figure 5), indicating that all these structures are dynamically stable. In the PHDOSs, there are two distinct frequency branches: the low-frequency vibrations below ~20 THz contributed by heavier Ti and P atoms and high-frequency vibrations mainly associated with H atoms. Figure S2 shows the phonon dispersion curves and PHDOSs of TiPH₁-P3m1, TiPH₃-Amm2, TiPH₅-I-4m2, TiPH₆-Cm, and TiPH₇-Cm, which confirm their dynamic stability.

In order to be used in experiment, structures of materials must have good mechanical stability. To examine the mechanical stabilities of TiPH_n, we calculated their elastic constants. The mechanical stability of hexagonal phase (e.g., TiPH₂-R-3m and TiPH₄-R-3m) should satisfy the criteria^[49]

$$C_{44} > 0, \quad C_{11} > |C_{12}|, \quad (C_{11} + 2C_{12})C_{33} > 2C_{13}^2 \quad (1)$$

and the criteria for mechanical stability of monoclinic phase (e.g., TiPH₈-C2/m)^[49] is given in the supporting information. Based on these criteria, all of TiPH₂-R-3m, TiPH₄-R-3m and TiPH₈-C2/m were mechanically stable, as seen from Table 1. At the

same time, the Young's modulus of TiPH₂-R-3m, TiPH₄-R-3m and TiPH₈-C2/m were compared with those of SH₃, PH₂, TiH₂, P, Ti, and TiP, showing that TiPH₄-R-3m and TiPH₈-C2/m have good elongation. Although their Young's modulus results do not reach the values of SH₃, they are more difficult to deform than the PH₂ and TiH₂ compounds, and thus the introduction of P atoms can improve the hydrogen embrittlement of the Ti-H compounds (Figure 6). This showed that these structures can be used in experiments, and their mechanical stability was sufficient to support their practical application without deformation.

Based on the stabilities and electronic properties of TiPH₂, TiPH₄ and TiPH₈, we predicted their T_c values at different pressures. The T_c calculation is accomplished by calculating electron-phonon coupling (EPC) parameter λ (Eq. 2), logarithmic average phonon frequency ω_{\log} , electronic density of states (DOS) at the Fermi level (ε_f), and Eliashberg phonon spectral function $\alpha^2F(\omega)$. $\alpha^2F(\omega)$ and λ are shown in Figure 7. λ and T_c are calculated by

$$\lambda = 2 \int_0^{\omega_b} \partial^2 F \frac{d\omega_q}{\omega_q} \quad (2)$$

and the Allen-Dynes modified McMillan equation^[50]

$$T_c = \frac{\omega_{\log}}{1.20} \exp \left[\frac{-1.04(1 + \lambda)}{\lambda(1 - 0.62\mu^*) - \mu^*} \right] \quad (3)$$

respectively. The T_c calculated values were given in Table 2.

From Figure 7, the total contributions from Ti and P atoms to T_c are 81% (250 GPa) for TiPH₂, 67% (100 GPa) and 60% (250 GPa) for TiPH₄, and 31% (250 GPa) for TiPH₈. Obviously, the heavy atoms contributed to T_c more than 80% in TiPH₂, whereas the H atoms contributed to T_c more than the Ti and P atoms in TiPH₄ and

TiPH₈. Too little hydrogen may be the main reason for the low T_c of TiPH₂ (calculated to be 2.22 K). The T_c of TiPH₄ calculated with μ* = 0.1 are 51.57, 38.08, 62.36, and 57.06 K at 100, 200, 250, and 300 GPa, respectively, highly promoted compared with the low T_c (4 K) of TiH_{2.74}^[41]. Though the T_c of TiPH₅ could reach 125 K at 250 GPa, the TiPH₅ is metastable based on the convex diagram (Figure S3). In addition, unlike the previously predicted P-H compounds, the TiPH and TiPH₄ compounds can be stabilized from 50 and 100 GPa on, respectively, which solves the instability of P-H compounds by adding Ti element and TiPH₄, which can be stabilized above 100 GPa, has also a high T_c, as mentioned above.

4. Conclusion

In this work, we systematically studied the structures and stabilities of TiPH_n (n = 1-8) at the pressure range 50-300 GPa. For the TiPH_n hydrides, we estimated their stabilities relative to two possible decompositions: TiPH_n → TiP + nH (n = 1-8) and TiPH_n → TiH₂ + P + (n-2)H (n = 2-8). From the convex diagram of the formation enthalpy of TiPH_n relative to TiPH_n → TiP + nH, TiPH is most stable at 50-200 GPa, TiPH₄ most stable at 250-300 GPa, and TiPH₈ can be stabilized above 200 GPa. Relative to TiPH_n → TiH₂ + P + (n-2)H (n = 2-8), TiPH₄ becomes most stable above 200 GPa, and TiPH₈ becomes stable above 200 GPa.

The calculated T_c of TiPH₄ R-3m phase are 51.57 and 62.36 K at 100 and 250 GPa, respectively, and the T_c of TiPH₈ C/2m structure was calculated to be 66.67 K at 250 GPa. By contrast, TiPH has no superconductivity and the calculated T_c of TiPH₂

at 250 GPa is only 2.22 K.

Ti-P-H hydrides have their own advantages: first, compared with unstable P-H compounds, the stability of TiPH_n ($n=1-8$) is significantly enhanced, secondly, Ti has a high affinity with H and thus H does not evaporate easily, On other hand, the problem of hydrogen embrittlement of Ti-H compound in experiment can be improved by adding P, and also T_c of Ti-P-H compounds was enhanced. Therefore, Ti-P-H materials could be expected to have potential applications in the field of superconducting materials.

Acknowledgments

This work was supported by the National Natural Science Foundation of China (Grant No. 21773132). Work at Ames Laboratory was supported by the U.S. Department of Energy, Office of Science, Basic Energy Sciences, Division of Materials Science and Engineering including the computer time support came from National Energy Research Scientific Computing Center (NERSC) in Berkeley, CA. Ames Laboratory is operated for the U.S. DOE by Iowa State University under Contract No. DE-AC02-07CH11358.

References

- [1] Bardeen, J.; Cooper, L. N.; Schrieffer, J. R. Microscopic Theory of Superconductivity *Phys. Rev.* **1957**, *106*, 162–164.
- [2] Ashcroft, N. W. Metallic Hydrogen: A High-temperature Superconductor? *Phys. Rev. Lett.* **1968**, *21*, 1748–1749.
- [3] Ashcroft, N. Hydrogen Dominant Metallic Alloys: High Temperature Superconductors? *Phys. Rev. Lett.* **2004**, *92*, 187002–187005.

- [4] Drozdov, A. P.; Eremets, M. I.; Troyan, I. A. Superconductivity above 100 K in PH₃ at high pressures *arXiv*: **2015**, 1508.06224.
- [5] Drozdov, A. P.; Eremets, M. I.; Troyan, I. A.; Ksenofontov, V.; Shylin, S. I. Conventional superconductivity at 203 K at high pressures in the sulfur hydride system *Nature*. **2015**, *525*, 73–76.
- [6] Geballe, Z. M.; Liu, H. Y.; Mishra, A. K.; Ahart, M.; Somayazulu, M.; Meng, Y.; Baldini, M.; Hemley, R. J. Synthesis and Stability of Lanthanum Superhydrides *Angew. Chem.* **2018**, *130*, 696-700.
- [7] Duan, D.; Liu, Y.; Tian, F.; Li, D.; Huang, X.; Zhao, Z.; Yu, H.; Liu, B.; Tian, W.; Cui, T. Pressure-induced metallization of dense (H₂S)₂H₂ with high-T_c superconductivity *Sci. Rep.* **2014**, *4*, 6968.
- [8] Liu, H.; Naumov, I. I.; Hoffmann, R.; Ashcroft, N. W.; Hemley, R. J. Potential high-T_c superconducting lanthanum and yttrium hydrides at high pressure *Proc. Natl. Acad. Sci. USA* **2017**, *114*, 6990.
- [9] Wang, H.; Tse, J. S.; Tanaka, K.; Iitaka, T.; Ma, Y. M. Superconductive sodalite-like clathrate calcium hydride at high pressures *Proc. Natl. Acad. Sci.* **2012**, *109*(17), 6463-6466.
- [10] Szczeńniak, R.; Durajski, A. P. The high-pressure superconductivity in SiH₄: The strongcoupling approach *Solid. State. Commun.* **2013**, *172*, 5–9.
- [11] Szczeńniak, R.; Drzazga, E. A.; Duda, A. M. The superconducting state in the B₂H₆ compound at 360 GPa, *Solid. State. Commun.* **2013**, *166*, 50–55.
- [12] Feng, X. L.; Zhang, J. R.; Gao, G. Y.; Liu, H. Y.; Wang, H. Compressed sodalite-like MgH₆ as a potential high-temperature superconductor *RSC Adv.* **2015**, *5*, 59292.
- [13] Li, Y. W.; Hao, J.; Liu, H.; Tse, J. S.; Wang, Y. C.; Ma, Y. M. Pressure-stabilized superconductive yttrium hydrides *Sci. Rep.* **2015**, *5*, 9948.
- [14] Olga D.; John E. P.; Christophe L. G.; Eugene G.; Michael H. Formation of transition metal hydrides at high pressures *Solid State Commun.* **2009**, *149*, 1583.
- [15] Szczeńniak, D.; Zemła, T. P. On the high-pressure superconducting phase in platinum hydride *Supercond. Sci. Technol.*, **2015**, *28*, 085018.

- [16]Eremets, M. I.; Trojan, I. A.; Medvedev, S. A.; Tse, J. S.; Yao, Y. Superconductivity in Hydrogen Dominant Materials: Silane *Science*, **2008**, 319, 1506.
- [17]Szczęśniak, R.; Durajski, A. P.; Szczęśniak, D. Study of the superconducting state in the Cmmm phase of GeH₄ compound *Solid State Commun*, **2013**, 165, 39-44.
- [18]Zhang, C.; Chen, X. Z.; Li, Y. L.; Struzhkin, V. V.; Hemley, R. J.; Mao, H. K.; Zhang, R. Q.; Lin, H. Q. Superconductivity in Hydrogen-rich Material: GeH₄ *J. Supercond. Nov. Magn.*, **2010**, 23, 717-719.
- [19]Alexander, G. K.; Dmitry, V. S.; Ivan, A. K.; Artem, R. O. High-Temperature Superconductivity in Th-H System at Pressure Conditions *ACS Appl. Mater. Interfaces*, **2018**, 10, 43809-43816.
- [20]Zhang, S.; Zhu, L.; Liu, H.; Yang, G. Structure and Electronic Properties of Fe₂SH₃ Compound under High Pressure *Inorg. Chem.* **2016**, 55, 11434.
- [21]Rahm, M.; Hoffmann, R.; Ashcroft, N. W. Ternary gold hydrides: Routes to stable and potentially superconducting compounds *J. Am. Chem. Soc.* **2017**, 139(25), 8740.
- [22]Ma, Y. B.; Duan, D. F.; Shao, Z. J.; Yu, H. Y.; Liu, H. Y.; Tian, F. B.; Huang, X. L.; Li, D.; Liu, B. B.; Cui, T. Divergent synthesis routes and superconductivity of ternary hydride MgSiH₆ at high pressure *Phy. Rev. B* **2017**, 96, 144518.
- [23]Fan, F.; Papaconstantopoulos, D. A.; Mehl, M. J.; Klein, B. M. High-temperature superconductivity at high pressures for H₃Si_xP_{1-x}, H₃P_xS_{1-x}, and H₃Cl_xS_{1-x} *J. Phys. Chem. Solids*. **2016**, 99, 105–110.
- [24]Muramatsu, T.; Wanene, W. K.; Somayazulu, M. Metallization and superconductivity in the hydrogen-rich ionic salt BaReH₉ *J. Phys. Chem. C* **2015**, 119, 18007.
- [25]Flores-Livas, J. A.; Amsler, M.; Heil, C.; Sanna, A.; Boeri, L.; Profeta, G.; Wolverton, C.; Goedecker, S.; Gross, E. K. U. Superconductivity in metastable phases of phosphorus-hydride compounds under high pressure *Phys. Rev. B* **2016**, 93, 020508.
- [26]Liu, H. Y.; Li, Y. W.; Gao, G. Y.; Tse, J. S.; Naumov, I. I. Crystal Structure and Superconductivity of PH₃ at High Pressures *J. Phys. Chem. C* **2016**, 120, 3458-3461.
- [27]Shamp, A.; Terpstra, T.; Bi, T.; Falls, Z.; Avery, P.; Zurek, E. Decomposition

Products of Phosphine Under Pressure: PH₂ Stable and Superconducting? *J. Am. Chem. Soc.* **2016**, *138*, 1884–1892.

[28]Chang, Y. H. *et al* Characterizing solute hydrogen and hydrides in pure and alloyed titanium at the atomic scale *Acta. Mater.* **2018**, *150*, 273-280.

[29]Deaven, D. M.; Ho, K. M. Molecular geometry optimization with a genetic algorithm *Phys. Rev. Lett.* **1995**, *75*, 288.

[30]Bush, T. S.; Catlow, C. R. A.; Battle, P. D. Evolutionary programming techniques for predicting inorganic crystal structures *J. Mater. Chem.* **1995**, *5*, 1269.

[31]Oganov, P.; Glass, C. W. Evolutionary crystal structure prediction as a tool in materials design *J. Phys-Condens. Mat.* **2008**, *20*, 064210.

[32]Perdew, J. P.; Chevary, J. A.; Vosko, S. H.; Jackson, K. A.; Pederson, M. R.; Singh, D. J.; Fiolhais, C. Atoms, molecules, solids, and surfaces: Applications of the generalized gradient approximation for exchange and correlation *Phys. Rev. B* **1992**, *46*, 6671-6687.

[33]Perdew, J. P.; Burke, K.; Ernzerhof, M. Generalized gradient approximation made simple *Phys. Rev. Lett.* **1996**, *77*, 3865–3868.

[34]Milman, V.; Winkler, B.; White, J. A.; Pickard, C. J.; Payne, M. C.; Akhmatkaya, E. V.; Nobes, R. H. Electronic structure, properties, and phase stability of inorganic crystals: a pseudopotential plane-wave study *Int. J. Quantum. Chem.* **2000**, *77*, 895-910.

[35]Qin, W.; Lu, W. C.; Xia, L. H.; Zhao, L. Z.; Zang, Q. J.; Wang, C. Z.; Ho, K. M. Theoretical study on the structures and optical absorption of Si₁₇₂ nanoclusters *Nanoscale.* **2015**, *7*, 14444.

[36]Zhao, L. Z.; Lu, W. C.; Su, W. S.; Qin, W.; Wang, C. Z.; Ho, K. M. Si₇₈ double cage structure and special optical properties *Phys. Chem. Chem. Phys.* **2015**, *17*, 27734.

[37]Yang, W. H.; Lu, W. C.; Ho, K. M.; Wang, C. Z. Hybrid silicon–carbon nanostructures for broadband optical absorption *RSC Adv.* **2017**, *7*, 8070.

[38]Dong, Y. H.; Lu, W. C.; Xu, X.; Zhao, X.; Ho, K. M.; Wang, C. Z. Theoretical search for possible Au-Si crystal structures using a genetic algorithm *Phys. Rev. B*

2017, 95, 134109.

[39]Wu, J.; Zhao, L. Z.; Chen, H. L.; Wang, D.; Chen, J. Y.; Guo, X.; Zang, Q. J.; Lu, W. C. 2018 Structures and Superconducting Properties of Ultra-Hydrogen-Rich Selenium Hydride H₆Se *Phys. Status. Solidi. B* **2018**, 255, 1800224.

[40]Giannozzi, P.; Baroni, S.; Bonini, N.; Calandra, M.; Car, R.; Cavazzoni, C.; Ceresoli, D.; Chiarotti, G. L.; Cococcioni, M.; Dabo, I. et al. QUANTUM ESPRESSO: a modular and open-source software project for quantum simulations of materials *J. Phys-Condens Mat.* **2009**, 21, 395502.

[41]Bashkin, I. O.; Nefedova, M. V.; Tissen, V. G.; Ponyatovskii, E. G. Superconductivity in the Ti-D system under pressure *Phys. Solid. State.* **1998**, 40, 1950–1952.

[42]Pickard, C. J.; Needs, R. J. Structure of phase III of solid hydrogen *Nat. Phys.* **2007**, 3, 473-476.

[43]Kikegawa, T.; Iwasaki, H. An X-ray diffraction study of lattice compression and phase transition of crystalline phosphorus *Acta Crystallogr., Sect. B* **1983**, B39, 158–164.

[44]Clark, S. M.; Zaug, J. M. Compressibility of cubic white, orthorhombic black, rhombohedral black, and simple cubic black phosphorus *Phys. Rev. B* **2010**, 82, 134111.

[45]Akahama, Y.; Kobayashi, M.; Kawamura, H. Simple-cubic-simple-hexagonal transition in phosphorus under pressure *Phys. Rev. B* **1999**, 59, 8520.

[46]Akahama, Y.; Kawamura, H.; Carlson, S.; Le, B. T.; Hausermann, D. Structural stability and equation of state of simple-hexagonal phosphorus to 280 GPa: Phase transition at 262 GPa *Phys. Rev. B* **2000**, 61, 3139.

[47]Jamieson, J. C. Crystal Structures Adopted by Black Phosphorus at High Pressures *Science.* **1963**, 139, 1291–1292.

[48]Gao, G. Y.; Bergara, A.; Liu, G. T.; Ma, Y. M. Pressure induced phase transitions in TiH₂, *J. Appl. Phys.* **2013**, 113, 103512.

[49]Wu, Z. J.; Zhao, E. J.; Xiang, H. P.; Hao, X. F.; Liu, X. J.; Meng, J. Crystal structures and elastic properties of superhard IrN₂ and IrN₃ from first principles *Phys.*

Rev. B **2007**, 76, 054115.

[50] Allen, P. B.; Dynes, R. C. Transition temperature of strong-coupled superconductors reanalyzed *Phys. Rev. B* **1975**, 12, 905.

Figure

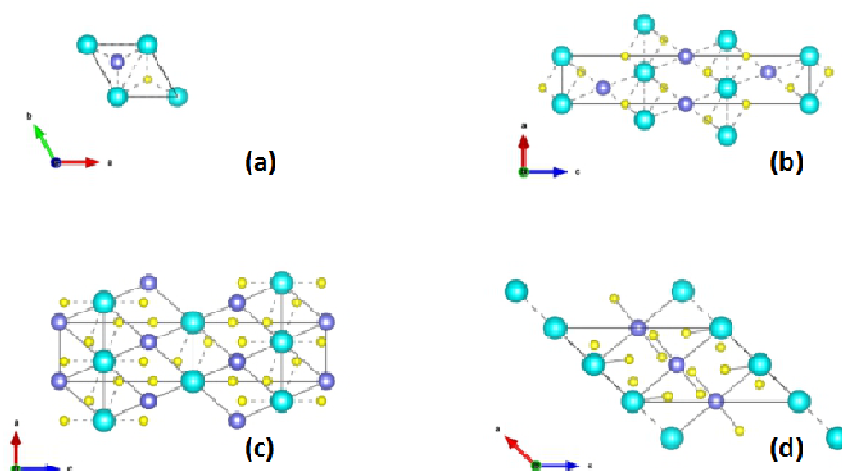


Fig. 1. Structures of TiPH , TiPH_2 , TiPH_4 and TiPH_8 at 250 GPa: (a) TiPH -P3m1 structure; (b) TiPH_2 -R-3m structure; (c) TiPH_4 R-3m structure; and (d) TiPH_8 C2/m structure. Blue, purple and yellow atoms represent Ti, P and H, respectively.

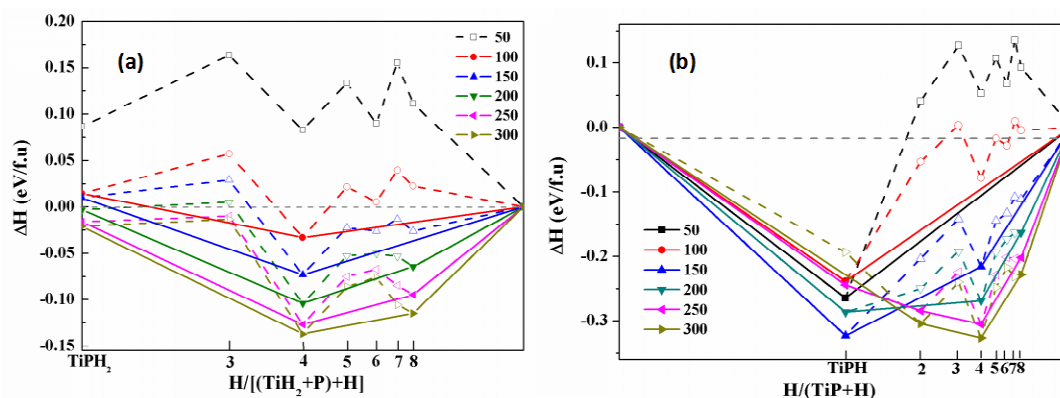


Fig. 2. Formation enthalpies of TiPH_n compounds: (a) formation enthalpies relative to decomposition $\text{TiPH}_n \rightarrow \text{TiP} + n\text{H}$ at 50-300 GPa; and (b) formation enthalpies relative to decomposition $\text{TiPH}_n \rightarrow \text{TiH}_2 + \text{P} + (n-2)\text{H}$ at 50-300 GPa. Solid shape points fall on the convex hull, which represent thermodynamically stable phases, while hollow shape points locate on dashed line, which denote metastable phase.

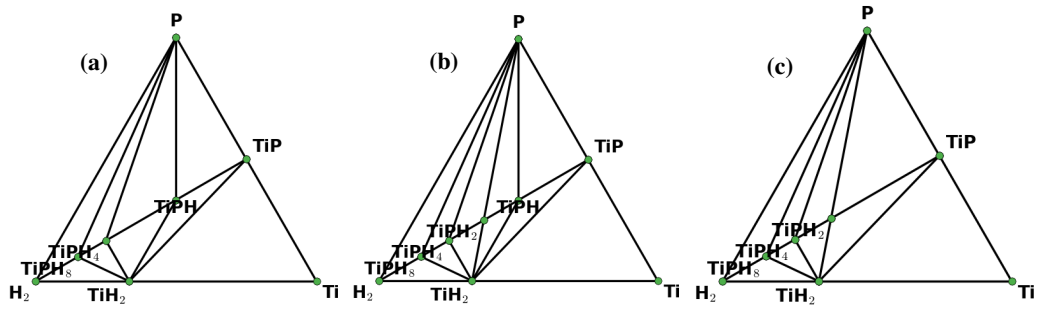


Fig. 3. Trigonal phase diagrams of the Ti-P-H compounds at 200, 250 and 300 GPa, respectively. Solid symbols denote stable stoichiometries.

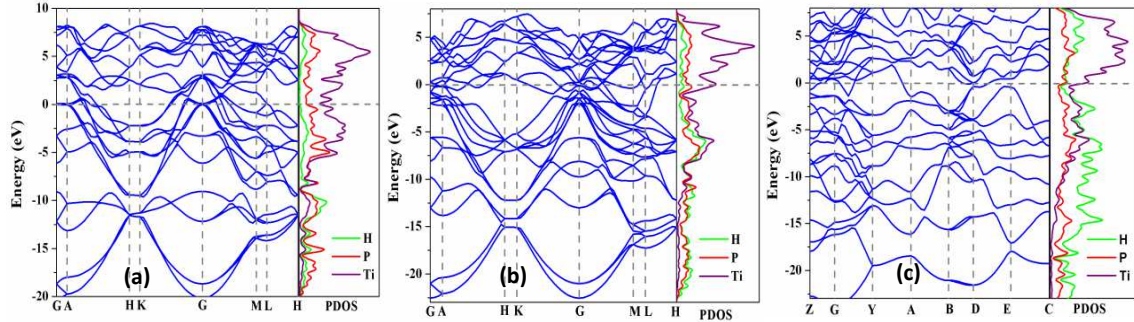


Fig. 4. Electronic band structures and PDOSs of (a) $\text{TiPH}_2\text{-R-3m}$, (b) $\text{TiPH}_4\text{-R-3m}$ and (c) $\text{TiPH}_8\text{-C2/m}$ at 250 GPa.

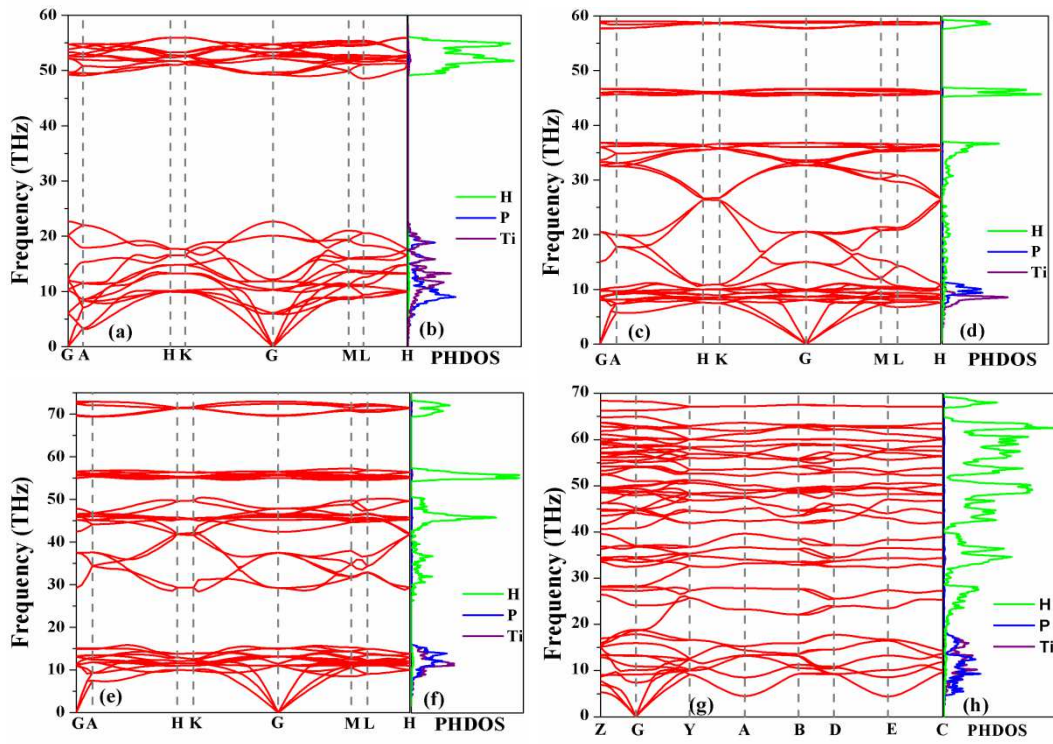


Fig. 5. (a), (c), (e) and (g) Calculated phonon dispersion curves of $\text{TiPH}_2\text{-R-3m}$ at 250 GPa, $\text{TiPH}_4\text{-R-3m}$ at 100 and 250 GPa and $\text{TiPH}_8\text{-C2/m}$ at 250 GPa. (b), (d), (f) and (h) Calculated PHDOSs of $\text{TiPH}_2\text{-R-3m}$ at 250 GPa, $\text{TiPH}_4\text{-R-3m}$ at 100 and 250 GPa and $\text{TiPH}_8\text{-C2/m}$ at 250 GPa.

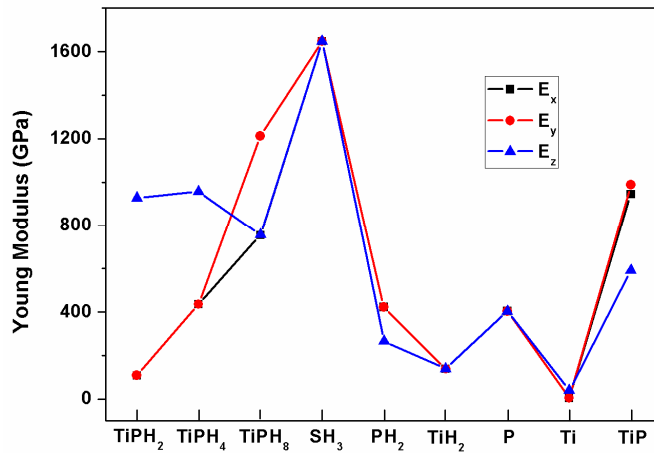


Fig. 6. Comparison of Young Modulus of TiPH_2 , TiPH_4 , and TiPH_8 with SH_3 , PH_2 , TiH_2 , P, Ti, and TiP on X, Y and Z axes.

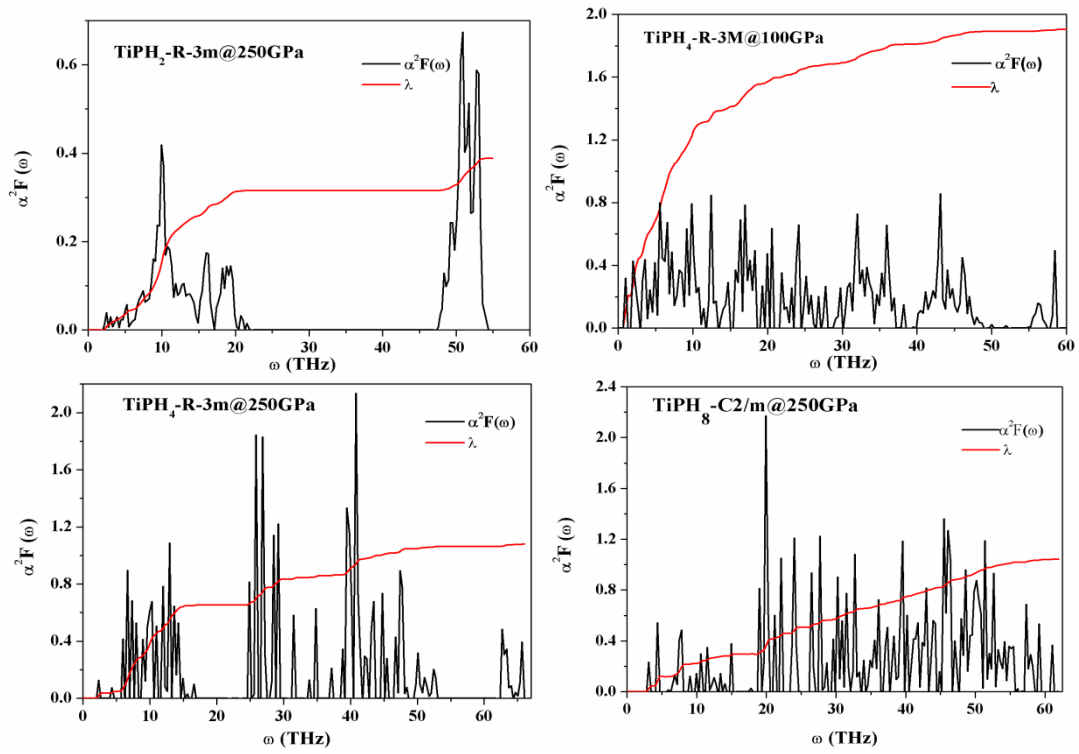


Fig. 7. Eliashberg phonon spectral function $\alpha^2 F(\omega)$, and electron-phonon coupling parameter λ of $\text{TiPH}_2\text{-R-3m}$ at 250 GPa, $\text{TiPH}_4\text{-R-3m}$ at 100 and 250 GPa, and $\text{TiPH}_8\text{-C2/m}$ at 250 GPa, respectively.

Table

	C ₁₁	C ₁₂	C ₁₃	C ₃₃	C ₄₄
TiPH ₂	947.84	843.23	794.14	1632.24	525.40
TiPH ₄	1118.09	859.47	634.85	1364.38	249.70
	C ₁₁	C ₁₂	C ₁₃	C ₁₅	C ₂₂
TiPH ₈	1155.31	537.30	647.46	0.47	1551.61
	C ₂₃	C ₂₅	C ₃₃	C ₃₅	C ₄₄
TiPH ₈	550.08	52.50	1166.84	9.00	274.87
	C ₄₆	C ₅₅	C ₆₆		
TiPH ₈	-83.73	214.45	315.98		

Tab. 1. Elastic stiffness constants C_{ij} for TiPH₂, TiPH₄ and TiPH₈.

	P (GPa)	ω_{\log} (K)	N (ϵ_f)	λ	T _c (K)	
					$\mu^* = 0.1$	$\mu^* = 0.13$
TiPH	150	749.031	2.191	0.131	0.00	0.00
TiPH ₂	250	624.512	14.155	0.389	2.22	0.91
TiPH ₃	250	197.246	14.870	2.239	30.51	28.66
	100	392.198	24.187	1.770	51.57	47.72
	200	340.640	22.832	1.470	38.08	34.65
	250	722.043	22.105	1.166	62.36	55.06
TiPH ₄	300	792.698	21.480	1.022	57.06	49.20
	250	908.452	13.762	1.901	126.06	117.25
	250	787.112	11.069	0.843	40.89	33.59
TiPH ₅	250	885.680	11.724	0.894	51.32	42.88
TiPH ₆	250	1009.756	11.886	0.967	66.67	56.80
	300	974.589	11.318	0.879	54.77	45.56

Tab. 2. Calculated EPC parameter λ , DOS at the Fermi level $N(\epsilon_f)$, logarithmic average phonon frequency ω_{\log} , and T_c of TiPH_n at different pressures.